Металлофиз. новейшие технол. / Metallofiz. Noveishie Tekhnol.
2015, т. 37, № 5, сс. 665–681
Оттиски доступны непосредственно от издателя
Фотокопирование разрешено только
в соответствии с лицензией

PACS numbers: 06.60.Vz, 62.20.Qp, 81.20.Vj, 81.40.Pq, 81.70.Bt, 81.70.Jb, 83.50.Uv

The Effects of Rotation Speed and Friction Time for Joining of AISI 4340–2205 Steels by Friction Welding

U. Caligulu, M. Yalcinoz*, N. Kati*, Z. Balalan**, and S. Islak***

Firat University, Faculty of Technology,
Department of Met. and Materials Eng.,
23119 Elazig, Turkey
**Firat University,*
Faculty of Technical Education,
Dept. of Metallurgy Education,
23119 Elazig, Turkey
***Bingol University,*
Faculty of Engineering,
Department of Met. and Materials Eng.,
12000 Bingol, Turkey
****Kastamonu University,*
Faculty of Eng. and Arch.,
Dept. of Mat. Sci. and Nanotech. Eng.,
Kastamonu, Turkey

Friction welding is a solid state joining process used extensively currently owing to its advantages such as low heat input, high production efficiency, ease of manufacture, and environment friendliness. Materials difficult to be welded by fusion welding processes can be successfully welded by friction welding. In the fusion welding methods for joining different materials, brittle intermetallic compounds phases are produced in the fusion zone, which reduces the strength of the welding joint. In this study, the effects of rotation speed and friction time for joining of AISI 4340–2205 steels welded by friction are investigated. Specimens of AISI 4340 tempered steel and AISI 2205 duplex stainless steel, each of 12 mm diameters, are used to fabricate the joints. The friction welding tests are carried out using a direct-drive type friction-welding machine, which was designed and manufactured for this purpose by us. After friction welding, in order to determine the occurred microstructural changes, the interface regions of the welded specimens are examined by means of OM, SEM, EDS and X-Ray analysis. Microhardness and tensile tests are conducted to determine the mechanical properties of the welded specimens. The experimental results indicate that AISI 4340 tempered steel could be joined to AISI 2205 duplex stainless steel using the friction welding technique and for achieving a weld with sufficient strength.

Tensile strength values also confirm this result, and, at the interface, intermetallic phases do not occurred. The maximum tensile strength of 635.66 MPa could be obtained for the joints welded under the welding conditions of rotation speed of 2200 rpm, friction pressure of 40 MPa, forging pressure of 80 MPa, friction time of 6 s, and forging time of 3 s.

Зварювання тертям являє собою процес твердотільного з'єднання, який в теперішній час інтенсивно використовується завдяки таким його перевагам, як низька підвідна теплота, висока продуктивність, простота реалізації та дружність до довкілля. Матеріяли, які важко з'єднуються зварюванням топленням, можуть бути успішно зварені зварюванням тертям. Методи зварювання топленням при з'єднанні різних матеріялів характеризуються утворенням в зоні стоплення фаз крихких інтерметалевих з'єднань, які знижують міцність зварного з'єднання. В даній роботі досліджується вплив швидкости обертання та часу тертя на з'єднання тертям сталей AISI 4340–2205. Зразки з відгартованої сталі AISI 4340 і двофазної неіржавійної сталі AISI 2205, кожний діяметром у 12 мм, використовувалися для виготовлення з'єднань. Випробування зварювання тертям виконувалися з використанням машини для зварювання тертям безредукторного типу, яку було сконструйовано та виготовлено нами для цього. Після зварювання тертям для визначення мікроструктурних змін в області розділчої межі зварених зразків використовувалися методи оптичної та сканувальної електронної мікроскопії, а також енергодисперсійна рентґенівська спектроскопія та рентґенодифракційний аналіз. Для визначення механічних властивостей зварених зразків виконувалися дослідження мікротвердости та випробування на розрив. Результати експериментів показують, що відгартована сталь AISI 4340 може з'єднуватися з двофазною неіржавійною сталлю AISI 2205 методою зварювання тертям з одержанням зварного шва достатньої міцности. Значення міцности на розрив також підтвердили цей результат і те, що в області контакту не виникають інтерметалеві фази. Максимальної міцности на розрив у 635,66 МПа було досягнуто для з'єднань, яких було одержано за наступних умов зварювання: швидкість обертання — 2200 об/хв., тиск тертя — 40 МПа, тиск пресування — 80 МПа, час тертя — 6 с, а час пресування — 3 с.

Сварка трением является процессом твердотельного соединения, который в настоящее время интенсивно используется благодаря таким его преимуществам, как низкая подводимая теплота, высокая производительность, простота реализации и дружественность по отношению к окружающей среде. Материалы, которые трудно соединяются сваркой плавлением, могут быть успешно сварены сваркой трением. Методы сварки плавлением при соединении различных материалов характеризуются образованием в зоне сплавления фаз хрупких интерметаллических соединений, которые снижают прочность сварного соединения. В настоящей работе исследуется влияние скорости вращения и времени трения на соединение трением сталей AISI 4340–2205. Образцы из отпущенной стали AISI 4340 и двухфазной нержавеющей стали AISI 2205, каждый диаметром 12 мм, использовались для изготовления соединений. Испытания сварки трением производились с использованием машины для сварки трением безредукторного типа, которая была сконструирована и изготовлена нами для

этой цели. После сварки трением для определения микроструктурных изменений в области границы раздела сваренных образцов использовались методы оптической и сканирующей электронной микроскопии, а также энергодисперсионная рентгеновская спектроскопия и рентгенодифракционный анализ. Для определения механических свойств сваренных образцов проводились исследования микротвёрдости и испытания на разрыв. Результаты экспериментов показывают, что отпущенная сталь AISI 4340 может соединяться с двухфазной нержавеющей сталью AISI 2205 методом сварки трением с получением сварного шва достаточной прочности. Значения прочности на разрыв также подтвердили этот результат и то, что в области контакта не образуются интерметаллические фазы. Максимальная прочность на разрыв 635,66 МПа была достигнута для соединений, полученных при следующих условиях сварки: скорость вращения — 2200 об/мин., давление трения — 40 МПа, давление прессования — 80 МПа, время трения — 6 с и время прессования — 3 с.

Key words: AISI 4340, AISI 2205, friction welding, rotation speed, friction time.

(*Received January 20, 2015*)

1. INTRODUCTION

Duplex stainless steel (DSS) is a well-known material for its excellent strength and corrosion resistance. However, joining DSS plates by the fusion welding causes significant reduction in the mechanical properties because of microstructure changes during weld solidification. It is very essential to maintain characteristics of the weld zone to use DSS in servicing highly critical environments, such as ocean mining machinery, oil and gas pipelines, desalination plants, chemical tankers of ships, *etc*. DSS has ferrite (α) and austenite (γ) in an approximately equal proportion, which possess body centred cubic (b.c.c.) and face centred cubic structure (f.c.c.) respectively [1]. During the controlled alloying process of the DSS under equilibrium conditions, ferrite-promoting elements (Cr, Mo, Mn, W, Nb, Si, Ti, and V) will concentrate by diffusion in the ferrite. At the same time, austenite-promoting elements (Ni, C, N, Co, and Cu) will concentrate by diffusion in the austenite phases. This gives the even formation of dual phase microstructure [2–3]. However, the welding of DSS forces the microstructure to remain in an excessive ferritic nature, because of the higher amounts of ferrite promoting elements in its chemical composition, and due to faster cooling rate. Austenite usually nucleates in the temperature range 1200–900°C. During cooling, the weld zone remains in this range of temperature for a very short period of time, *i.e.* from 4 s to 15 s. Thus, the arc energy and filler metal composition play a major role in microstructural stability after welding [4].

Tempered types of steel are machinery manufactured steels with and

without alloy, whose chemical compositions, especially in terms of carbon content, are suitable for hardening and which shows high toughness under a specific tensile strength at the end of the tempering process. Tempered types of steel, due to their superior mechanical properties, acquired at the end of the tempering process, are used in a wide range including the manufacture of parts such as various machine and engine parts, forging parts, various screws, nuts and stud bolts, crankshafts, shafts, control and drive components, piston rods, various shafts, gears. For this reason, tempered steels are the type of steel used and produced at the highest rate after the unalloyed steels and construction steels. These steels constitute the most important part of the machinery-manufacturing steels. Generally, such steels are used for the production of fitting, axle shaft, the shaft and the gear [5–9].

Friction welding is a solid state joining process, which can be used to join a number of different metals. The process involves making welds in which one component is moved relative to, and in pressure contact, with the mating component to produce heat at the faying surfaces. Softened material begins to extrude in response to the applied pressure, creating an annular upset. Heat is conducted away from the interfacial area for forging to take place. The weld is completed by the application of a forge force during or after the cessation of relative motion. The joint undergoes hot working to form a homogenous, full surface, high-integrity weld. Friction welding is the only viable method in this field to overcome the difficulties encountered in the joining of dissimilar materials with a wide variety of physical characteristics. The advantages of this process are, among others, no melting, high reproducibility, short production time and low energy input [10–20].

Urena [21] developed the optimum welding condition for joining 2205 DSS using plasma–arc welding. Ku *et al.* [22] welded 2205 duplex stainless steel by electron beam welding and analysed the mechanical properties, microstructure and corrosion properties of the weldment. Kannan and Murugan [23] observed the effects of FCAW process parameters on DSS clad quality. Laser beam welding parameters were optimized by Reisgen *et al.* [24] and they found that, RSM can be considered as a powerful tool in experimental welding optimization. As the weld bead quality depends on the process parameters, it is essential to study the effects of process parameters on weld quality. Dobrovidov [25] investigated the selection of optimum conditions for the friction welding of high speed steel to carbon steel. Ishibashi *et al.* [26] chose stainless steel and high-speed steel as representative materials with an appreciably difficult weldability, and their adequate welding conditions were established. The distributions of the alloying elements at and near the weld interface with sufficient strength were investigated using X-ray microanalysis. Mumin Sahin [9–10] analysed the variations in hardness and microstructure at the interfaces of friction weld-

ed steel joints. While using austenitic stainless steel, negative metallurgical changes like delta ferrite formation and chromium carbide precipitation between grain boundaries took place during fusion welding. These changes were eliminated by friction welding. The effect of friction time on the fully plastically deformed region in the vicinity of the weld was investigated by Sathiya *et al.* [27]. Ananthapadmanaban *et al.* [28] reported the effect of friction welding parameters on tensile properties of steel. Satyanarayana *et al.* [29] joined austenitic–ferritic stainless steel (AISI 304 and AISI 430) using continuous drive friction welding and investigated optimum parameters, microstructures-mechanical property and fracture behaviours. Yilmaz [30] investigated the variations in hardness and microstructures in the welding zone of friction welded dissimilar materials. Paventhan *et al.* [31] investigated optimization of friction welding process parameters for joining carbon steel and stainless steel.

In this study, the objective of the present work is to examine the effects of rotation speed and friction time for joining of AISI 4340–2205 steels by friction welded.

2. EXPERIMENTAL

AISI 4340 tempered steel and AISI 2205 duplex stainless steel of 12 mm diameter were used to fabricate the joints in this study. Table 1 illustrates the chemical compositions of the base metals. The friction-welding tests were carried out using a direct-drive type friction-welding machine. Table 2 was given mechanical properties and Table 3 was given physical properties of AISI 4340 and AISI 2205 steels. Table 4 illustrates the experimental conditions. The experimental set-up is

TABLE 1. Chemical compositions of test materials.

Materials	Alloy Elements (% wt.)									
	C	Mn	Si	P	S	Cr	Mo	Ni	N	Cu
AISI 4340	0.4	0.8	0.3	0.035	0.040	0.9	0.3	2.00	–	–
AISI 2205	0.018	1.686	0.309	0.026	0.003	22.333	3.379	4.932	0.191	0.097

TABLE 2. Mechanical properties of copper and low carbon steel.

Materials	Tensile Strength, MPa	Yield Strength 0,2%, MPa	Elongation, %	Microhardness, HV
AISI 4340	659	400	20,98	201
AISI 2205	956	620	20	328

TABLE 3. Physical properties of copper and low carbon steel; α—thermal expansion coefficient (20–800°C), λ—thermal conductive (20°C), ρ—electrical resistance (20°C), *E*—elastic modulus (20°C).

Materials	α, 10^{-6} K^{-1}	λ, W/(m·K)	ρ, nΩ·m	*E*, GPa
AISI 4340	12.3	44.5	248	190–200
AISI 2205	14.7	19	85	200

TABLE 4. The process parameters used in the friction welding.

Sample No.	Welding parameters					
	Rotating speed, rpm	Friction pressure, MPa	Forging pressure, MPa	Friction time, s	Forging time, s	Axial shortening, mm
S1	2200	40	80	6	3	4.50
S2	2200	40	80	10	5	4.78
S3	2100	40	80	6	3	3.44
S4	2100	40	80	10	5	3.96
S5	2000	40	80	6	3	2.20
S6	2000	40	80	10	5	2.60

shown in Fig. 1.

After friction welding procedure, specimens were divided into sections transversely in order to investigate the microstructural variations from the centre to the outside of the weld. Transverse sections

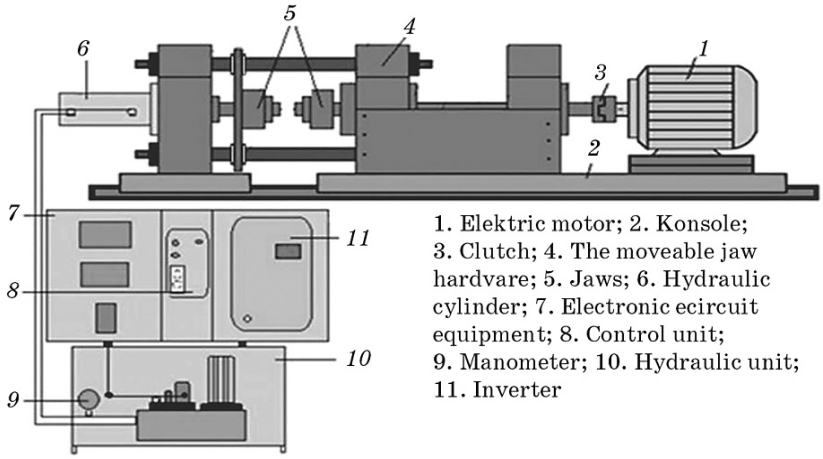

Fig. 1. Experimental set-up [17].

were prepared, and then, grinding and polishing 3 μm diamond paste were made in order to conduct metallographic examination of the joined materials.

The specimens were etched chemical in a solution for AISI 4340 2% HNO_3 + 98% Alcohol and in a solution for AISI 2205 25% HNO_3 + 75% pure water to conduct the microstructural examination (7.5 V + 30 s) The microstructures of the joints were observed using Optical Microscopy (OM), the Energy Dispersive Spectroscopy (EDS) and X-Ray Diffraction (XRD). Microhardness measurements were taken under a load of 50 g. Tensile tests were conducted at room temperature with 10^{-2} mm·s^{-1} crosshead rate.

3. RESULTS AND DISCUSSION

3.1. Microstructure

The macroview of specimens S1, S2, S3, S4, S5, and S6 welded under different welding conditions is shown in Fig. 2. Visual examination of the welded specimens showed uniform weld joints. As it can be seen in Fig. 2, the amount of flash increases with an increase in friction time, friction pressure, and rotation speed. In the case that the dissimilar materials are joined using the friction welding method, the formation of the flash depends on the mechanical properties of two parent materials. Maximum post-welding axial shortening is measured 4.78 mm on S2 specimen.

The flash obtained was symmetric, which indicated plastic deformation on both the rotating and upsetting (reciprocating) side. The integrity of the joints was evaluated for the friction-welded joints. The friction-processed joints were sectioned perpendicular to the bond line and observed through an OM microscope. It can be clearly seen that, there were no crack and voids in the weld interface.

From the microstructural observations, the microstructures formed

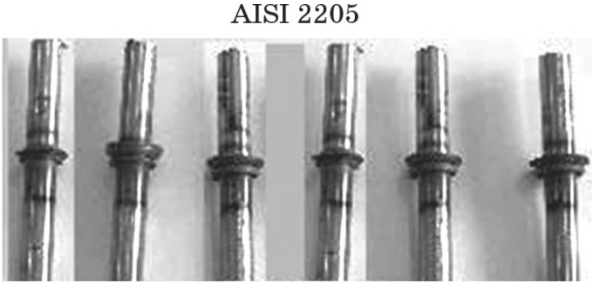

Fig. 2. Overview of friction welded AISI 4340–AISI 2205 steels.

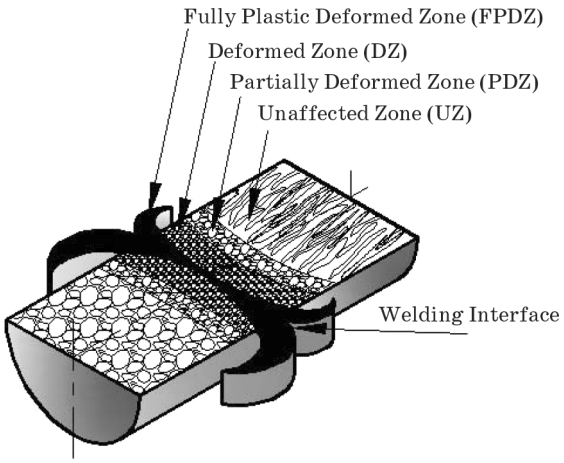

Fig. 3. Regions, which occurred microstructural chances [32].

interface zone during or after FW processes, there are three distinct zones across the specimens identified as unaffected zone (UZ), deformed zone (DZ) and transformed and recrystallized fully plastic deformed zone (FPDZ). Typical grain refinement occurred in the DZ region by the combined effect of thermal and mechanical stresses (Fig. 3). A typical micrograph showing the different morphologies of the microstructure at different zones of the friction processed joint is shown in Fig. 3.

It was observed that the rotational speed had an effect on geometry and width of the weld zone. The mechanical deformation and the frictional heat at the interface that dissipated through the parent materials results in a temperature gradient causing zones of materials with different microstructure. Although this condition causes lower cooling rates and a wider heat affected zone (HAZ), higher rotational speed leads narrower FPDZ due to a greater volume of viscous material transferred out of at the interface. It is a known fact that when pressure is used to bring joint pair together by plastic deformation results in dynamic recrystallization leading to a grain refinement in the central region of the weld. The effect of increasing rotational speed on the friction welded joint is an increase in both temperature gradient and axial shortening as a result of more mass being transferred out of the welding interface. High rotational speed can cause local heating at the interface, thus reaching a high temperature in a short time. This condition causes lower cooling rates and a wider HAZ, as a consequence of a greater volume of viscous material transferred out of the interface. AISI 4340 tempered steel was greatly deformed by the severe plastic deformation and frictional heat near the weld zone. There were no blanks, cracks or porosities in the weld was determined (Fig. 4).

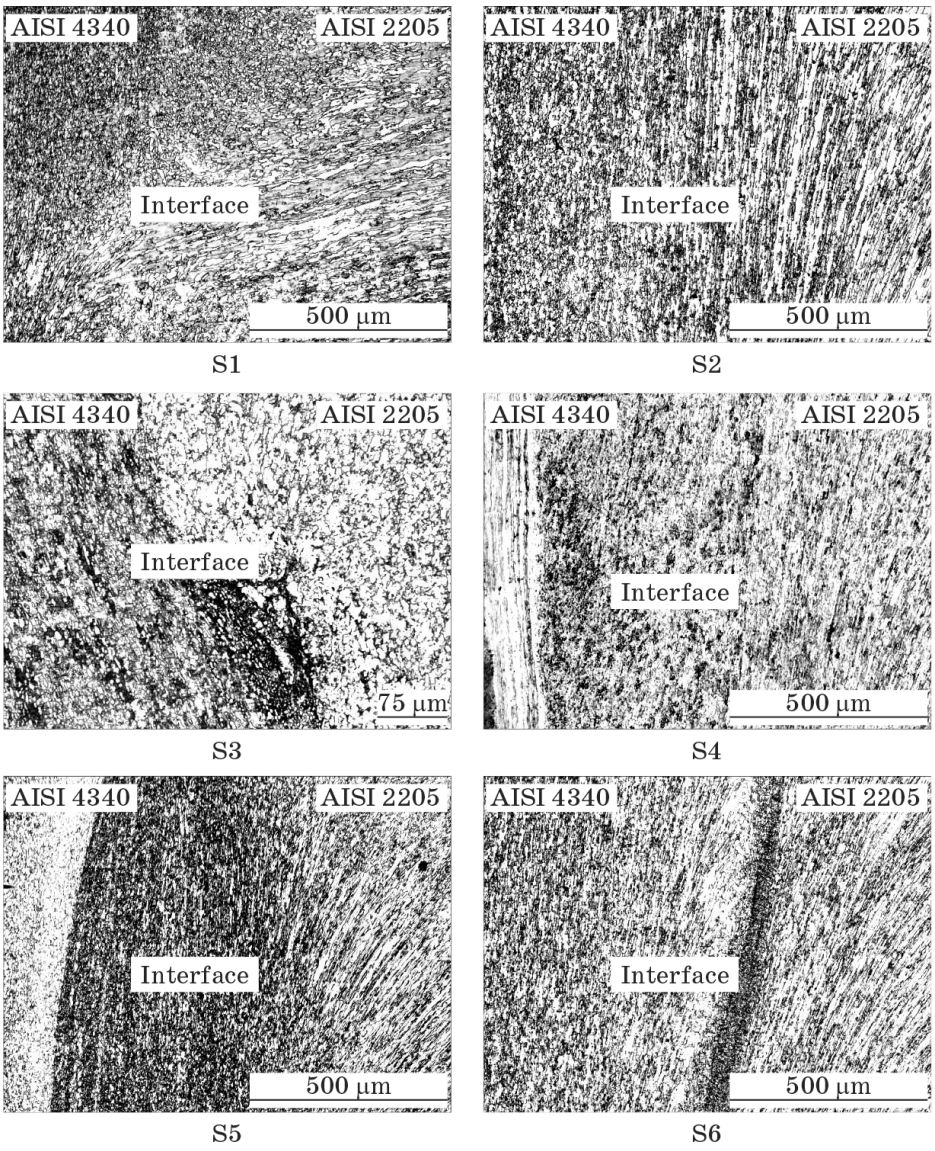

Fig. 4. Optical micrograph taken from the welding interface of the specimens S1, S2, S3, S4, S5, and S6, respectively.

During the friction welding process, the temperature at the interface was measured by IGA 15 PLUS detector, and the temperature values at interface of the joints are given in Fig. 5. It shows the temperature that occurred at the interface of the joint comes close to melting point of AISI 4340 tempered steel (1065–1198°C), which can reach between A3 temperature and the melting point of AISI 4340 tempered

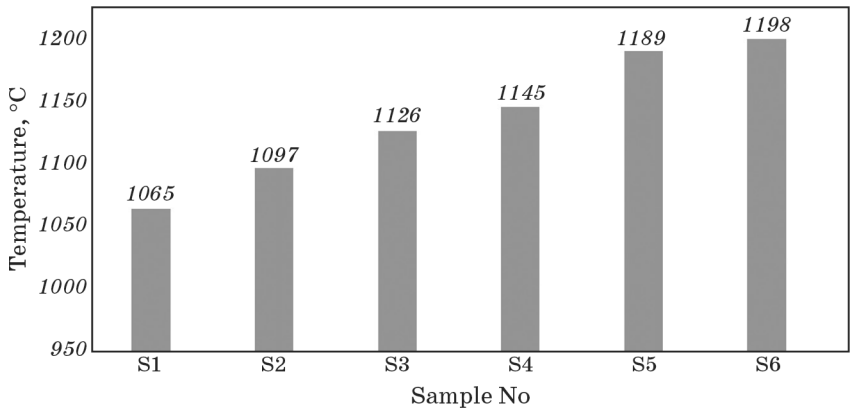

Fig. 5. The temperature at the interface of FW joints.

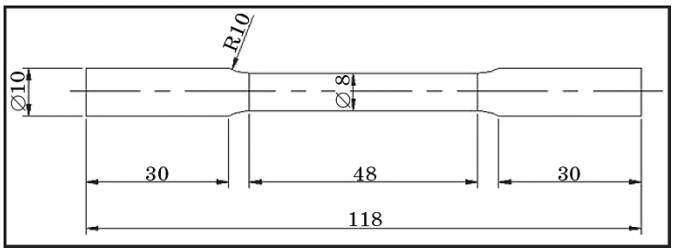

Fig. 6. Shape and measurement of the tensile test specimens [33].

Fig. 7. Macrophoto of tensile test results of friction-welded joints.

steel.

3.2. Tensile

Shape and measurements of the tensile specimens were seen in Fig. 6. The results of tensile tests were given in Figs. 7 and 8, respectively. As

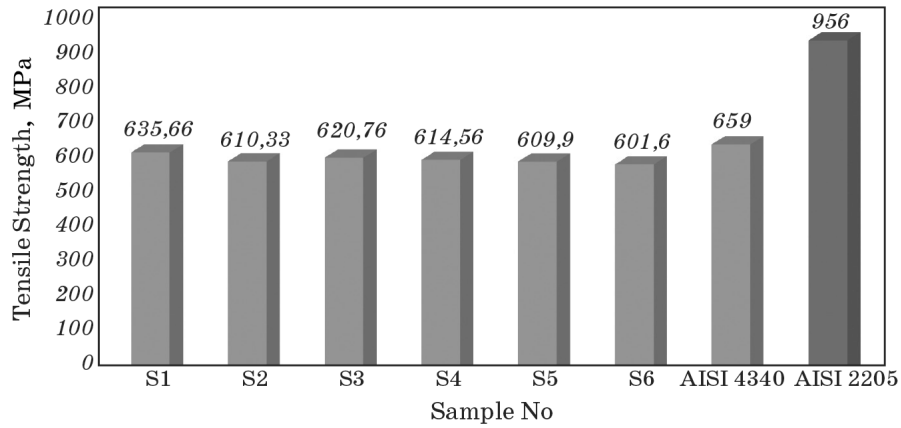

Fig. 8. Tensile test results of friction-welded joints.

it is clearly seen in Fig. 8, the tensile strength slightly increased while the rotation speed increased. Results of the tensile tests concluded that all joints were fractured by necking at the tempered steel side (see Fig. 7).

Current studies in literature report that a higher bonding temperature results in profuse interdiffusion and better coalescence of mating surfaces.

Plastic deformation detected in the specimens after the welding was not observed. However, increasing bonding temperature due to the increase of the rotational speed and the friction time also promotes the growth of brittle intermetallic, which adversely affects the bond strength in turn. Therefore, low elongation and strength values can be attributed to presence of aligned tempered steel precipitation reducing these properties. Maximum tensile strength and minimum temperature of the FW joints was achieved at the rotational speed of 2200 rpm in S1, 635.66 MPa and 1065°C, respectively.

This increase in tensile strength was related to the heat input and high plastic deformation occurring at the component interface as a result of the rotational speed and the axial pressure. Minimum tensile strength and maximum temperature of FW joints was obtained at 2000 rpm in specimen S6, 601.60 MPa and 1198°C, respectively. This decrease in tensile strength was associated with the reactions taking place at the HAZs of the tempered steel side. Longer time intervals allowed thermal energy to propagate along the axial direction of the work materials, and as a consequence, a bulk volume of material was heated. Therefore, longer time intervals led to lower cooling rates and a wider HAZ. As the friction time decreased, the joining efficiency steeply increased, and reached a maximum value at the rotational speed of 2200 rpm for 6 s with 635.66 MPa and then decreased again.

Under given conditions (2200, 2100, and 2000 rpm rotation speeds), tensile strengths were close to parent material, and slightly increased at increased rotation speeds.

3.3. Fractography

Figure 9 shows the images of the fracture surfaces resulting from the tensile test for the friction-welded specimens S1 and S6. Examining the fracture surface images, fractures resulting from the tensile test were mostly on the AISI 4340 tempered steel side, and it was observed that the fracture surface contains ductile dimples, formed by the microvoid coalescence mechanism and facets associated with the cleavage fracture. The dimples are believed to initiate at the second-phase particles or small inclusions within the ferrite and austenite phase of the AISI 2205 duplex stainless steel, whereas the facets represent brittle fracture occurring along the cleavage planes of the phase. As illustrated in Fig. 9, the number of ductile dimples increases with decreasing rotation speed. This type of fracture topography is classified as the

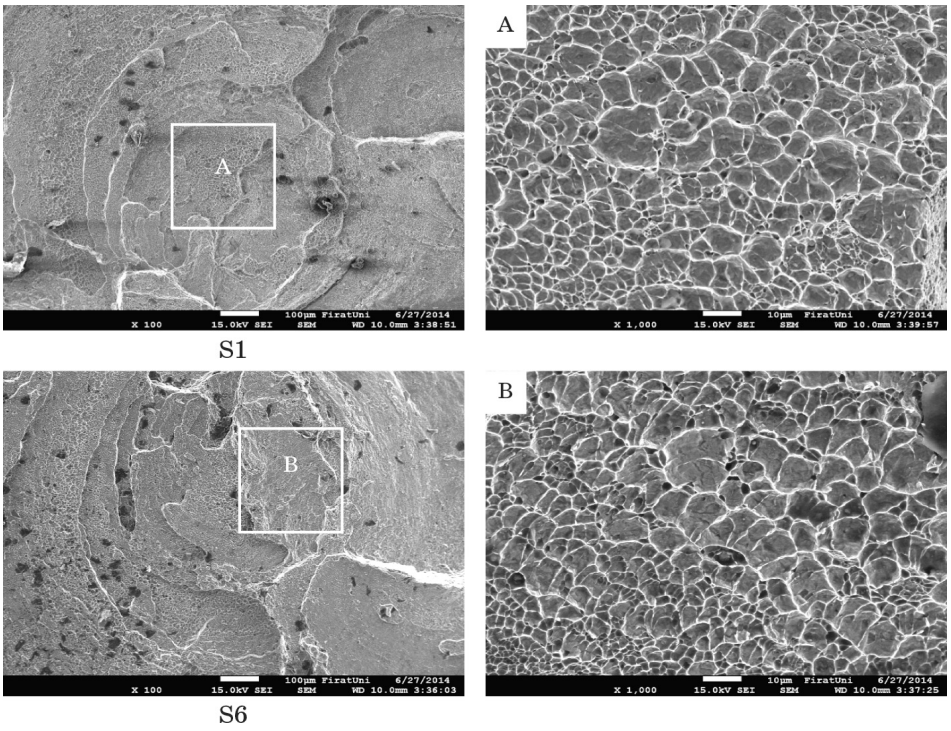

Fig. 9. Micrograph of the tensile fracture surfaces of S1 and S6 specimens observed by SEM.

quasi-cleavage. In generally, mechanism of ductile fracture was observed in the samples.

3.4. Microhardness

Microhardness measurements in the direction perpendicular to the weld interface of the friction-welded joints for specimens S1–S6 are given in Figs. 10 and 11.

As seen in these figures, a significantly similar trend is observed in the microhardness profiles of all specimens.

The increasing hardness in the welding interface can be directly associated with the microstructure in the welding interface as a result of the increasing heat input and severe plastic deformation. Microhardness values can be increased with increasing the rotational speed and friction time. This can be explained with the C, Cr, Mn, Fe, and Ni dif-

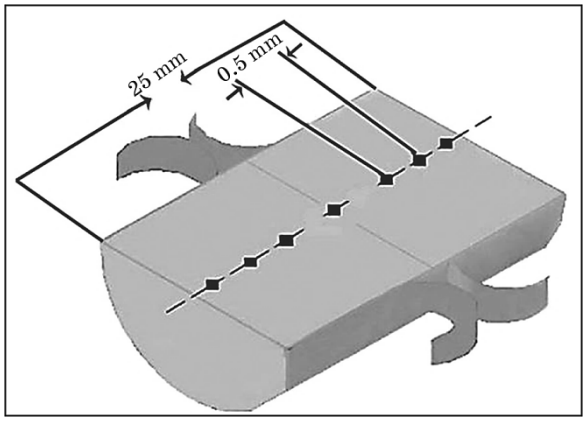

Fig. 10. Schematic illustration of microhardness distribution across the welding interface [33].

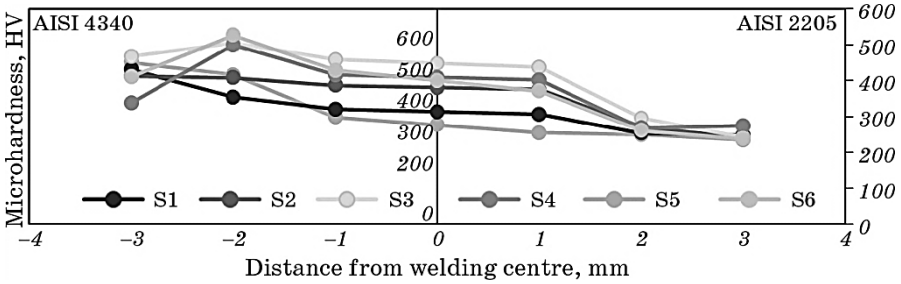

Fig. 11. Microhardness distribution across the welding interface of friction-welded specimens.

fusion of parent materials at weld interface, thus it has relatively lower hardness. The increase in the hardness in the AISI 4340 side can be attributed to the work hardening of the duplex stainless steel. Besides, the main reason for this is associated with the temperature increase in the interface, which is caused by deformation and friction. The temperature increase caused by the increase in the friction time enhances the viscosity of the material in the interface and enables its quick removal out of the interface. The increase in the upset time, on the other hand, is thought to create a forging effect on the AISI 4340 side and cause an increase in hardness.

3.5. X-Ray Diffraction and EDS Analysis

Figure 12 illustrates X-Ray diffraction across the interface of the S1 specimen. In the X-Ray analysis, like Fe–Ni, Fe–Cr–Ni, Fe–Cr, $Cr_{23}C_6$, Cr–Fe–Ni–C, and Cr_7C_3 phases were determined (Fig. 12). In the EDS analysis, as well as C, Cr, Mn, Fe, and Ni elements, non-intermetallic phases determined in the welding interface were detected. In the 60 μm distance, from AISI 4340 tempered steel to AISI 2205 duplex stainless steel, Fe, C, and Mn diffusion, and in equal distance from AISI 2205 duplex stainless steel to AISI 4340 tempered steel, Cr and Ni diffusion occurred (Table 5 and Fig. 13).

The frictional heat generated at the interface (under identical welding conditions) would be high for low-density elements due to their high boundary friction coefficients and low thermal conductivity compared to high-density elements. The welding procedure made with dis-

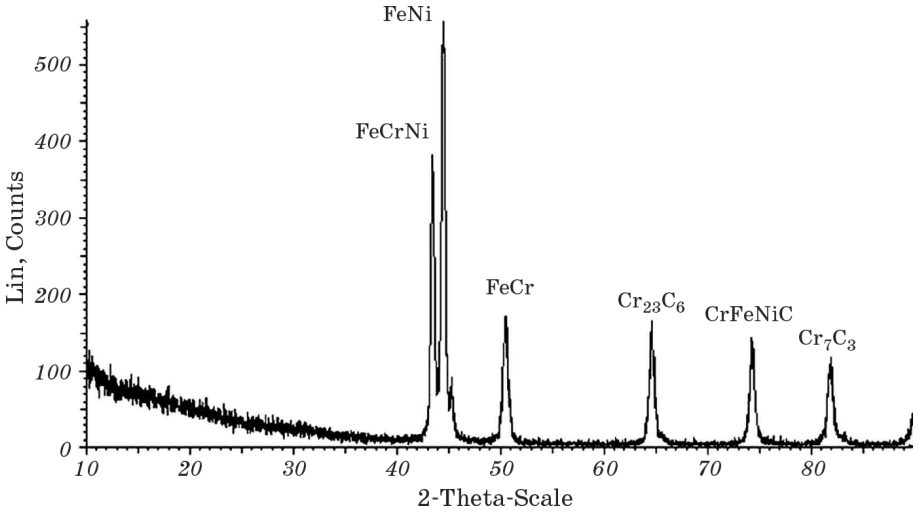

Fig. 12. The result of XRD analyses of S1 specimen.

TABLE 5. Values of concentrations taken from EDS analyses across the welding interface of S1 specimen.

EDS point	Alloying elements, % wt.				
	C	Cr	Mn	Fe	Ni
1	11.15	11.56	1.22	71.73	4.34
2	14.13	3.46	0.74	80.57	1.10
3	17.18	1.01	0.74	78.83	2.24

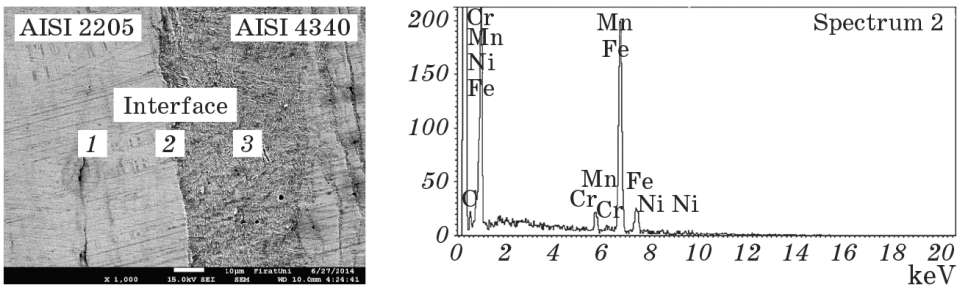

Fig. 13. EDS analyses across the welding interface of the friction-welded specimen S1.

similar materials exhibits wider plasticized zone in the middle of the welding interface. As for low-density elements, content of intermixing elements is higher in comparison to high-density elements. This is caused by the fact that higher flow required for the high-density elements restricts movement comparing to the low-density elements, which can move freely.

4. CONCLUSION

AISI 4340 tempered steel and AISI 2205 duplex stainless steel were joined by friction technique using different process parameters. Conclusions drawn based on the results of microstructure analysis, hardness, and tensile tests are presented below.

This study concluded that AISI 4340 tempered steel could be joined according to Table 4 successfully to AISI 2205 duplex stainless steel using the friction welding technique. Comprehensive microstructural investigations for AISI 4340–2205 friction-welded joints revealed that there are different regions at the welding interface, the width of fully plasticized deformed zone decreases when rotational speed and friction pressure increase.

The higher microstructural changes take place in the HAZs. An in-

crease in the contraction of the samples is observed after increasing the friction welding rotation speeds. The width of HAZ is mainly affected by friction time and rotation speed. This infers that the width and formation of HAZs, which occurred as a result of the reactions taking place at the welding interface, have an adverse effect on the mechanical strength and, consequently, the quality of the friction-welded joints.

The highest deformation was always at AISI 4340 tempered steel side, and in all samples, the original structure was preserved in the undeformed region.

A rotation speed of 2000 rpm was not completely sufficient to join AISI 4340–2205 steels by friction welding, but a rotation speed of 2200 rpm was sufficient for joining these materials.

The maximum tensile strength of 635.66 MPa could be obtained for the joints welded under the welding conditions of rotation speed of 2200 rpm, friction pressure of 40 MPa, forging pressure of 80 MPa, friction time of 6 s and forging time of 3 s. All samples were subjected to tensile testing showed brittle characteristics of the fracture topography in the partially deformed region on the AISI 4340 steel side (Fig. 8).

The increase in hardness at the HAZs is attributed to the microstructural transformation that occurs during the friction welding process. The strengthening effect observed in this region is mostly a direct result of the rapid cooling from the welding temperature. For achieving a welding with a sufficient strength, the friction time has to be held as short as possible, while the rotational speed has to be as high as possible (Fig. 11).

In the X-Ray analysis, Fe–Ni, Fe–Cr–Ni, Fe–Cr, $Cr_{23}C_6$, Cr–Fe–Ni–C, and Cr_7C_3 phases were determined. In the EDS analysis, nonintermetallic phases determined in the welding interface were detected, as well as C, Cr, Mn, Fe, and Ni elements.

REFERENCES

1. *ASM Handbook on Welding* (Eds. K. Ferjutz and J. R. Davis), vol. **6**, p. 471 (1993).
2. J. Charles, *Proc. of 7th Duplex Int. Conf. and Expo* (Grado: 2007).
3. J. C. Lippold and D. J. Kotecki, *Welding Metallurgy and Weldability of Stainless Steels* (Hoboken, NJ: Wiley-Interscience: 2005).
4. A. V. Jebaraj and L. Ajaykumar, *Indian Journal of Engineering and Materials Sciences*, No. 21: 155 (2014).
5. S. D. Meshram, T. Mohandas, and G. Madhusudhan Reddy, *J. Mater. Processing Technol.*, **184**, Iss. 1–3: 330 (2007).
6. P. Sathiya, S. Aravindan, and A. Noorul Haq, *Materials and Design*, **29**, Iss. 6: 1099 (2008).
7. S. Celik and I. Ersozlu, *Material Design*, **30**, Iss. 4: 970 (2009).

8. http://www.celmercelik.com.
9. M. Sahin and H. E. Akata, *Indust. Lubricat. Tribol.*, **56**, No. 2: 122 (2004).
10. M. Sahin, *Materials and Design*, **28**: 1348 (2007).
11. I. Kirik and N. Ozdemir, *Int. J. Mater. Res.*, **104**, No. 8: 769 (2013).
12. N. Ozdemir, F. Sarsilmaz, and A. Hascalik, *Material Design*, **28**, Iss. 1: 301 (2007).
13. *Welding Handbook. Vol. 2. Welding Processes* (8th Ed.) (Miami: American Welding Society Inc.: 1997), No.739–761.
14. R. E. Chalmers, *Manufacturing Engineering*, No. 126: 64 (2001).
15. N. Ozdemir, *Mater. Lett.*, **59**, Iss. 19–20: 2504 (2005).
16. D. E. Spindler, *Welding Journal*, **73**, No. 3: 37 (1994).
17. I. Kirik, N. Ozdemir, and U. Caligulu, *Kovove Materials*, No. 51: 4 (2013).
18. I. Kirik, N. Ozdemir, and F. Sarsilmaz, *MP Material Testing*, No. 54: 10 (2012).
19. M. B. Uday, M. N. Ahmad Fauzi, H. Zuhailawati, and A. B. Ismail, *Sci. Technol. Welding and Joining*, No. 15: 7 (2010).
20. J. Domblesky and F. F. Kraft, *J. Mater. Process. Technol.*, **191**, Iss. 1–3: 82 (2007).
21. A. Urena, E. Otero, M. V. Utrilla, and C. J. Múnez, *J. Mater. Process. Technol.*, **182**, Iss. 1–3: 624 (2007).
22. J. S. Ku, N. G. Ho, and S. C. Tjong, *J. Mater. Process. Technol.*, **63**, Iss. 1–3: 770 (1997).
23. T. Kannan and N. Murugan, *J. Mater. Process. Technol.*, **176**, Iss. 1–3: 230 (2006).
24. U. Reisgen, M. Schleser, O. Mokrov, and E. Ahmed, *Optic Laser Technology*, **44**, Iss. 1: 1 (2012).
25. A. N. Dobrovidov, *Weld Prod.*, No. 22: 3 (1975).
26. A. Ishibashi, S. Ezoe, and S. Tanaka, *Bulletin of the JSME*, No. 26: 216 (1983).
27. P. Sathiya, S. Aravindan, and A. Noorul Haq, *Int. J. Adv. Man. Tech.*, **26**, Iss. 5–6: 505 (2005).
28. D. Ananthapadmanaban, V. Seshagiri Rao, Nikhil Abraham, and K. Prasad Rao, *Materials and Design*, **30**, Iss. 7: 2642 (2009).
29. V. V. Satyanarayana, G. Madhusudhan Reddy, and T. Mohandas, *J. Materials Processing Technology*, No. 160: 2 (2005).
30. M. Yilmaz (Istanbul: Technical University of Yildiz: 1993).
31. R. Paventhan, P. R. Lakshminarayanan, and V. Balasubramanian, *J. Iron and Steel Research, International*, **19**, Iss. 1: 66 (2012).
32. S. Mercan and N. Ozdemir, *NWSA: Technological Applied Sciences*, No. 8: 2 (2013).
33. N. Kati and S. Ozan, *New World Science Academy (NWSA)*, **2A0086**, No. 9 (3): 22 (2014).